Applied Catalysis B: Environmental 129 (2013) 89–97

Contents lists available at SciVerse ScienceDirect

Applied Catalysis B: Environmental

journal homepage: www.elsevier.com/locate/apcatb

Photocatalytic degradation of 2,4,6-tribromophenol over Fe-doped $ZnIn_2S_4$: Stable activity and enhanced debromination

Bo Gao*, Lifen Liu*, Jiadong Liu, Fenglin Yang

Key Laboratory of Industrial Ecology and Environmental Engineering, MOE, School of Environmental Science and Technology, Dalian University of Technology, Dalian 116024, PR China

ARTICLE INFO

Article history:
Received 21 May 2012
Received in revised form 28 August 2012
Accepted 9 September 2012
Available online 18 September 2012

Keywords:
Zerovalent iron nanoparticles
Band gap
Photocatalysis
LC MS

ABSTRACT

Fe doped $ZnIn_2S_4$ catalyst was prepared and tested for photocatalytic degradation of 2,4,6-tribromophenol (2,4,6-TBP), it was more efficient in debromination and total organic carbon (TOC) removal, compared with TiO_2 (P25) and $ZnIn_2S_4$. The preparation of Fe-$ZnIn_2S_4$ involved a facile hydrothermal $ZnIn_2S_4$ synthesis process at low temperature and without templates, followed by chemical reductive deposition of Fe. The catalysts were characterized using scanning electron microscopy (SEM) equipped with an X-ray energy dispersive spectroscopy (EDS), TEM and HRTEM, FT-IR spectra, X-ray diffraction (XRD) and UV–vis diffuse reflectance spectra. The band gaps of $ZnIn_2S_4$ and Fe-$ZnIn_2S_4$ calculated from the onset of the absorption edges were 2.12 eV and 2.05 eV, respectively. The calculated pseudo-first-order constants (K_r) were in the order of TiO_2 ($0.022\,min^{-1}$) < 0.5 wt% Fe-TiO_2 ($0.0369\,min^{-1}$) < $ZnIn_2S_4$ ($0.362\,min^{-1}$) < 0.5 wt% Fe-$ZnIn_2S_4$ ($0.436\,min^{-1}$). After 1 h reaction by Fe-$ZnIn_2S_4$, the released bromide concentration was $17.6mg\,l^{-1}$, which was 1.11 and 2.69 times higher than $ZnIn_2S_4$ and TiO_2 (P25), respectively. The increase in TOC removal was 7% and 33% compared to $ZnIn_2S_4$ and TiO_2 (P25), respectively. The repeated tests proved that the synthesized Fe-$ZnIn_2S_4$ was stable, reusable and durable in degradation of 2,4,6-TBP. The possible cycle of iron species and a tentative debromination pathway were proposed.

1. Introduction

Brominated phenols are present in the environment as intermediates or end-products from industrial manufacturing processes. An enormous number of brominated phenols, especially 2,4,6-tribromophenol (2,4,6-TBP), are manufactured as multipurpose brominated flame retardant, reactive intermediates, pesticides/wood preservatives and important pharmaceutical intermediates. Brominated phenols are of great potential to contaminate aquatic environment due to their wide use, low naturally occurring degradation and higher water solubility (15 °C, dissolve in water, 1/14,000). The presence of brominated phenols in water causes serious problems on account of their toxicity, suspected carcinogenicity and adverse effects on the thyroid hormone system in animals and human beings [1]. The stable C—Br bond in BPs is responsible for their toxicity and persistence, so breaking the C—Br bond and debromination are crucial for toxicity reduction. Recently, in order to reduce the toxicity of BPs, various degradation processes such as biological degradation [1], electrochemical process and photocatalytic degradation [2,3] have been studied. However, biological degradation requires long period and pure bacterial strain. Photocatalytic process is one of the most promising technologies for removal of persistent organic pollutants for the high degradation rate and non-selective oxidation. But the high degree of recombination of photogenerated electrons and holes and the low photocatalytic activity limited the application of single semiconductor photocatalysts, the development of nanocomposite photocatalysts has received lots of attentions. The TiO_2 composites doped with quantum dots [4] and iron (including zero valent iron) [5–7] have shown very attractive features, such as enhanced dehalogenation and enhanced mineralization of pollutants.

Low-cost and effective zerovalent iron nanoparticles (ZVI NPs) have been proved with high conversion efficiency of halogen compounds to less toxic products [8]. However, the consumption of nanoscale Fe^0 and production of iron sludge are drawbacks for the application of ZVI NPs. Moreover, the unsupported particles are unstable and prone to agglomeration, which lead to reactivity reduction of ZVI NPs. Immobilizing the NPs onto supports without compromising the surface reactivity of ZVI NPs in mitigating the agglomeration of ZVI NPs has been studied [9,10]. The

Abbreviations: 2,4,6-TBP, 2,4,6-tribromophenol; DBP, dibromophenol; BP, bromophenol; MB, methylene blue; ZVI NPs, zerovalent iron nanoparticles; NZVI, nanoscale zerovalent iron.

* Corresponding authors. Tel.: +86 411 84706173; fax: +86 411 84708083.
E-mail addresses: gbljd1986@163.com (B. Gao), yuzhe25521@yahoo.com.cn (L. Liu).

0926-3373/$ – see front matter © 2012 Elsevier B.V. All rights reserved.
http://dx.doi.org/10.1016/j.apcatb.2012.09.007

ZVI NPs on TiO_2 was proved able to enhance the dechlorination efficiency and reduce recombination rate of photogenerated electrons and holes, which effectively decolorized azo dye [5], and in the presence of nickel ions, enhanced the dechlorination efficiency of trichloroethylene [6] and the coupled dechlorination of trichloroethylene and 2,4-dichlorophenol [7]. The reductive Fe and Fe/Pd bimetallic nanoparticles were immobilized in polymer film for reductive degradation of TCE [11]. In our recent study, both the powder Fe^0-TiO_2 nanocomposites and the composite membrane with Fe^0-TiO_2 and activated carbon fiber enhanced the photocatalytic degradation of 2,4-dichlorophenol [12,13]. It is interesting and worthy to study the photocatalytic debromination using Fe^0-TiO_2 and composites of ZVI with other photocatalysts and their debromination performance.

Ternary sulfide $ZnIn_2S_4$, as a visible light photocatalyst with a layered structure, has a band gap for broader sunlight absorption. $ZnIn_2S_4$ nanotubes and nanoribbons, nanowires and microspheres had been prepared through a facile solution-based route by Gou et al. [14]. Photoelectrochemical properties of $ZnIn_2S_4$ film electrodes had been investigated [15]. It had also been used in splitting water for hydrogen production [16] and photoelectrocatalytic inactivation of *E. coli* [17]. $ZnIn_2S_4$ nano/micropeonies, synthesized via a simple hydrothermal method and microwave-solvothermal process, efficiently degraded dyes under visible light [18]. $ZnIn_2S_4$ showed high and stable photocatalytic activity for water reduction [19] and Cu-doping enhanced its photocatalytic activity in hydrogen evolution [20]. It is anticipated that $ZnIn_2S_4$, especially the micro-peony $ZnIn_2S_4$ with nanolamella petals, a good candidate for supporting VZI NPs, would have excellent photocatalytic activity in debromination. In this study, ZVI NPs were immobilized onto $ZnIn_2S_4$ support, assisted in effective and efficient photocatalytic debromination of 2,4,6-tribromophenol for toxicity reduction and even complete mineralization. TiO_2 (P25) and Fe-TiO_2 were also tested for comparison purposes.

2. Experimental

2.1. Materials

2,4,6-tribromophenol (AR) and methylene blue (AR) were supplied by Sinpharm Chemical Reagent Co., Ltd. The initial concentration of 2,4,6-TBP was 0.12 mmol l^{-1} and the initial pH was 6.89. The concentration of methylene blue was 50 ppm and the pH was 7.77. Other reagents such as $Zn(NO_3)_2{\cdot}6H_2O$, $In(NO_3)_3{\cdot}5H_2O$, CH_3CSNH_2 (TAA), $FeSO_4{\cdot}7H_2O$ and $NaBH_4$ were of analytical grade. The commercial Degussa P25 was used as the standard TiO_2 sample. All materials were used as received without further purification. The water used in this test was ultrapure water with the specific resistance of 18.2 MΩ cm.

2.2. Preparation of $ZnIn_2S_4$, Fe-$ZnIn_2S_4$ and Fe-TiO_2

In a typical and simple procedure, 0.25 mmol $Zn(NO_3)_2{\cdot}6H_2O$ and 0.5 mmol $In(NO_3)_3{\cdot}5H_2O$ and an excessive CH_3CSNH_2 (TAA, 4 mmol) were dissolved in 50 ml deionized water and then transferred to a 70 ml Teflon-lined autoclave. The autoclave was sealed and maintained at 80 °C for 6 h and then allowed to cool to ambient temperature naturally. The yellow product was collected by centrifugation at 10,000 rpm for 5 min, and then washed twice with deionized water and finally dried at 60 °C in vacuum for 10 h.

Fe-TiO_2 and Fe-$ZnIn_2S_4$ were synthesized via chemical reduction using $NaBH_4$. 1 g of $ZnIn_2S_4$ or TiO_2 was dispersed in 50 ml of 0.1 M $FeSO_4{\cdot}7H_2O$ under an inert nitrogen atmosphere. After stirring 30 min, 0.1 M $NaBH_4$ (20% excess) was added dropwise to ensure the complete reduction of Fe(II) to Fe^0. Then the solution was kept stirring for another 30 min under the inert nitrogen atmosphere. The precipitate was separated by centrifugation at 10,000 rpm for 5 min and washed three times with deionized water and then dried in vacuum for further characterization and photocatalytic reaction. For comparison, the $ZnIn_2S_4$ without ferrous doping was treated with the same excess $NaBH_4$, which marked as R-$ZnIn_2S_4$. Four series of Fe-$ZnIn_2S_4$ were prepared, where the weight ratio of Fe to $ZnIn_2S_4$ were 0.25%, 0.5%, 1.0% and 1.5%. 0.5 wt% Fe-TiO_2 was prepared as a comparison catalyst.

2.3. Photocatalytic activity measurements

The UV-light and visible light photocatalytic activities of the samples were investigated by degradation of TBP and MB, respectively, in an aqueous solution at room temperature. The photocatalytic reactor was a cylindrical quartz tube with a dimension of 3 cm × 30 cm (diameter × height). The distance between the reactor and the lamp was 10 cm. The UV light source was a 20 W germicidal low-pressure mercury lamp with main wavelength of 254 nm and the light intensity was 297 μW/cm^2 (with Al reflector surrounding the reactor and the lamp). Visible light source was a 100 W Tungsten-Halogen and the light intensity was 1925 mW/cm^2. A 50 mg of the catalyst powder (TiO_2, Fe (0.5%)-TiO_2, $ZnIn_2S_4$ or Fe (0.5%)-$ZnIn_2S_4$) and 100 ml of TBP or MB solution were added into the quartz reactor from the top portion of the tube and subjected to aeration (0.1 l min^{-1}) for thorough mixing and suspension. The adsorption experiments were carried out in the dark and the photocatalytic experiments were carried out under UV light and/or visible light.

5 ml reaction suspension was withdrawn at specific time intervals and filtered through 0.22 μm millipore (acetate cellulose) filter and then analyzed. The ultraviolet-visible spectrophotometer (Shimadzu, UV-1700) was used to detect the changes of MB during the photocatalytic process. The concentration of 2,4,6-TBP was determined by high performance liquid chromatography (HPLC, Shimadzu, VP-ODS, 150L × 4.6), in which a mobile phase of methanol and water was employed (80:20, v/v) at a flow rate of 1.0 ml min^{-1}, an injection volume of 5 μl was used and the UV detector wavelength was set at 295 nm. Samples were collected after the reaction and centrifuged at 12,000 rpm for 10 min to measure the extent of mineralization of 2,4,6-TBP by a total organic carbon (TOC) analyzer (TOC-TN vcp Shimadzu). The released Br^- was measured according to the method for determining bromine content in groundwater (F-HZ-DZ-DXS-0062, China). The data reported were average of three tests and the error bars represented the standard deviation. The liquid chromatography-electron spray ionization mass spectrometry (LC-ESI MS, Agilent Technologies) was used to determine the debromination intermediates. Chromatographic analysis was carried out with a mixture of 40% ultrapure water supplemented with 0.2% formic acid and 60% acetonitrile. The flow rate was 0.25 ml min^{-1} and 5 μl of the extracted samples were injected.

2.4. The stability study of Fe-$ZnIn_2S_4$

25 mg 0.5 wt% Fe-$ZnIn_2S_4$ catalyst was mixed into 50 ml of 2,4,6-TBP solution and then irradiated under UV light for 1 h. After the 1st run, the suspension was centrifuged at 12,000 rpm for 10 min to recover the suspended catalysts. The supernatant was used to analyze the concentration of 2,4,6-TBP and the bromine content. The collected catalysts were dispersed in 50 ml fresh 2,4,6-TBP solution to carry out the second run. In this way, the experiments were repeated for 6 times. When the 7th cyclic experiment was completed, the catalyst was collected in a 10 ml sampling bottle to carry out another seven-cycle experiment after two months.

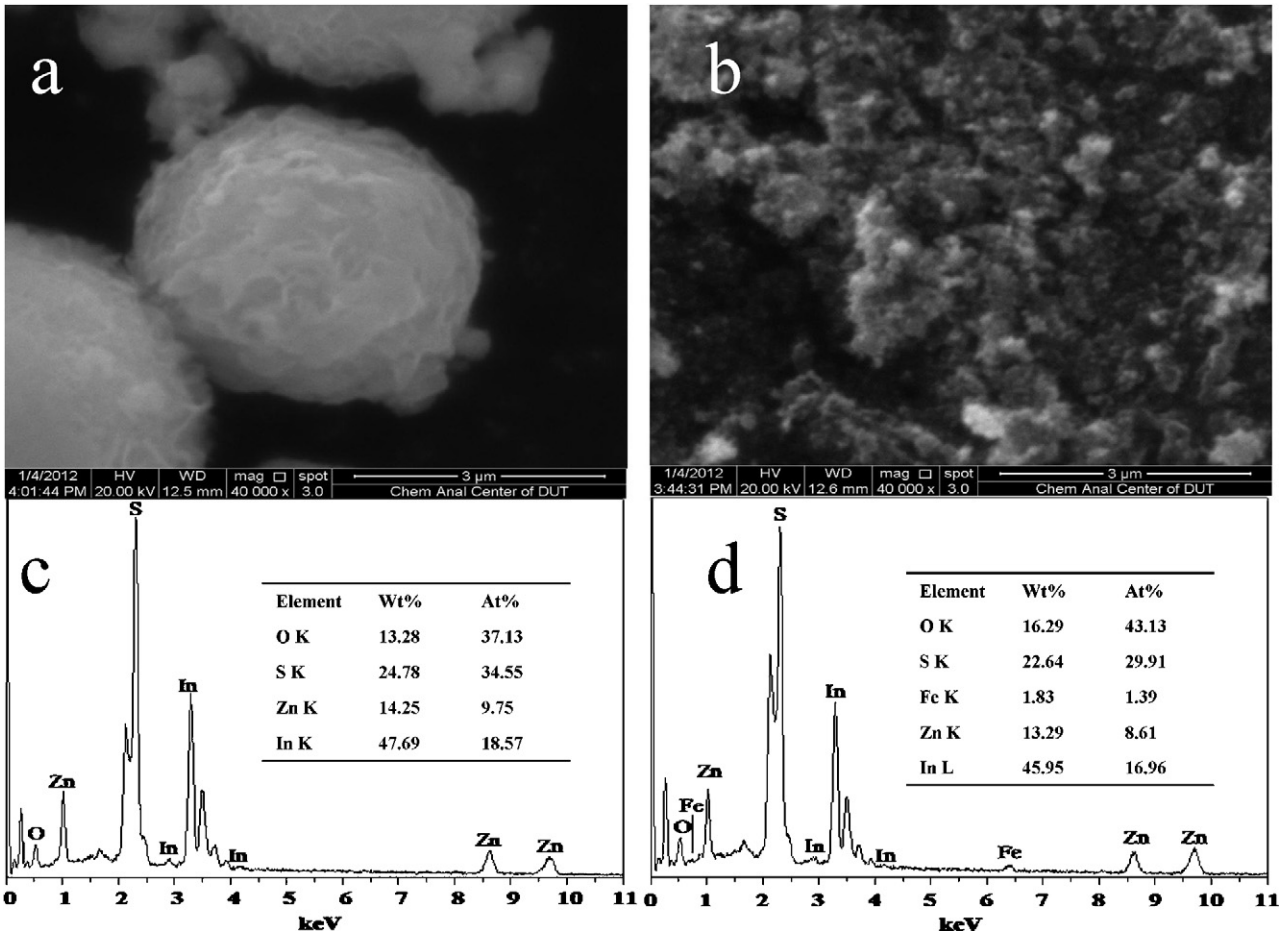

Fig. 1. SEM images and EDS analysis of $ZnIn_2S_4$ (a and c) and 1.5 wt% Fe-$ZnIn_2S_4$ composite (b and d).

2.5. Characterization

The morphology was characterized using a scanning electron microscopy (SEM, NOVA NANOSEM450, USA) equipped with an X-ray energy dispersive spectroscopy (EDS). Transmission electron microscopy (TEM-100CX-II) and high-resolution TEM (HRTEM) analyses were operated at an accelerating voltage of 200 kV. The Brunauer–Emmett–Teller (BET) surface areas were measured by nitrogen adsorption and desorption at 77.3 K. The crystal structures of the particles were characterized by powder X-ray diffraction (XRD) using Cu Kα (λ = 1.5406 Å) radiation at a scanning speed of 4°/min ranging from 10° to 80°. The accelerating voltage and applied current were 40 kV and 100 mA, respectively. The optical properties of the prepared samples were measured by a UV-Vis spectrophotometer (JASCO Corp., V-550). IR spectra were obtained using IRPrestige-21 FT-IR spectrophotometer (SHIMADZU).

3. Results and discussion

3.1. Characterization

3.1.1. Morphology

The morphology of $ZnIn_2S_4$ without Fe was shown by the separate microspheres (average diameter, 3–5 μm) and all the microspheres had lamellar structures with numerous nanosheets or nanopetals (Fig. 1a). This lamellar microsphere structure was related to the layered structure of hexagonal $ZnIn_2S_4$ [21]. After doping 1.5% Fe^0, the layered structure was hardly observed in Fe-$ZnIn_2S_4$ (Fig. 1b), which might be attributed to the chemical reduction by $NaBH_4$. The space inside the $ZnIn_2S_4$ microsphere might be hollow structure [22] which was easily destructed by the chemical reduction. As shown in Supplementary data, S1, the lamellar structured microsphere was not observed for R-$ZnIn_2S_4$ ($ZnIn_2S_4$ treated with $NaBH_4$). This demonstrated that chemical reduction was the major reason for the change of the morphology.

The elemental composition of the as-prepared catalysts $ZnIn_2S_4$ and Fe-$ZnIn_2S_4$ were shown by EDS elemental mapping (Fig. 1c and d). The three main feature elements Zn, In and S were detected on the surface of the two catalysts. The EDS analysis from SEM images clearly showed the peak of Fe in the Fe-$ZnIn_2S_4$ composite and the content of Fe in the particle surfaces was 1.83%. The intended weight ratio of Fe loading on $ZnIn_2S_4$ was ~1.5%. The difference between the calculated (intended) value and the measured value revealed that the nanoscale Fe^0 particles were unevenly distributed in the composites and almost all the Fe^0 particles were on the surface.

In the TEM images of $ZnIn_2S_4$ (Fig. 2a and b), some unequal nanopetals were assembled in the fringe of the microsphere, the measured length of the distinguishable and transparent nanopetals was ~200 nm. When Fe^0 was introduced to $ZnIn_2S_4$ (Fig. 2d and e), the nanosheets at the microsphere edge shrank and the measured thickness of the distinguishable microsphere edge was ~120 nm. The unequal nanopetals were reduced and formed more regular and smoother microsphere edge, which probably related to the chemical reduction. From the HRTEM image in Fig. 2c, the lattice interplanar spacing was measured to be ~0.325 nm, corresponding to the (1 0 2) plane of hexagonal $ZnIn_2S_4$ [21]. The lattice interplanar spacing of Fe doped $ZnIn_2S_4$ (Fig. 2f) was measured to be

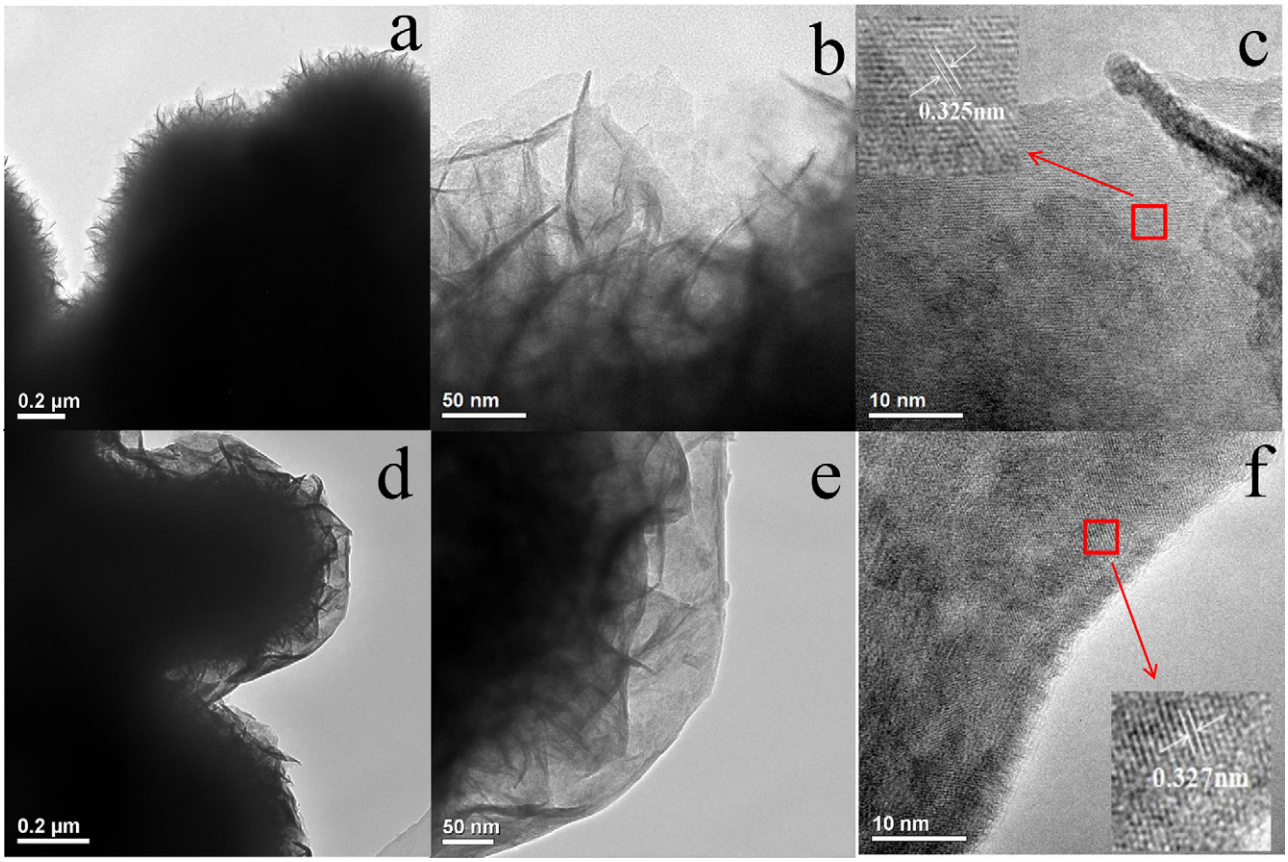

Fig. 2. Low-magnification TEM, high-magnification TEM, HRTEM of $ZnIn_2S_4$ (a, b, c) and Fe-doped $ZnIn_2S_4$ composite (e, f, g).

~0.327 nm, indicating doping Fe^0 did not affect the crystal structure of $ZnIn_2S_4$.

3.1.2. XRD analysis

The crystallographic structure and phase of the samples were determined by XRD. The XRD patterns of $ZnIn_2S_4$ and Fe-$ZnIn_2S_4$ samples were shown in Fig. 3. All the diffraction peaks of the obtained $ZnIn_2S_4$ can be indexed as the reflection of the hexagonal phase of $ZnIn_2S_4$, which were consistent with the observations of other literatures [23]. The XRD patterns revealed that the introduction of nanoscale Fe^0 did not change the crystal phase, meaning the doped Fe did not incorporate into the lattice of the $ZnIn_2S_4$. The characteristic diffraction peak of zero valent Fe should be at $2\theta = 44.64^\circ$ [12], but there was no zero valent Fe peak in the XRD pattern of 1.5 wt% Fe-$ZnIn_2S_4$ sample because the doping amount of zero valent Fe was low. Fe was detected and shown through the EDS elemental mapping (Fig. 1d).

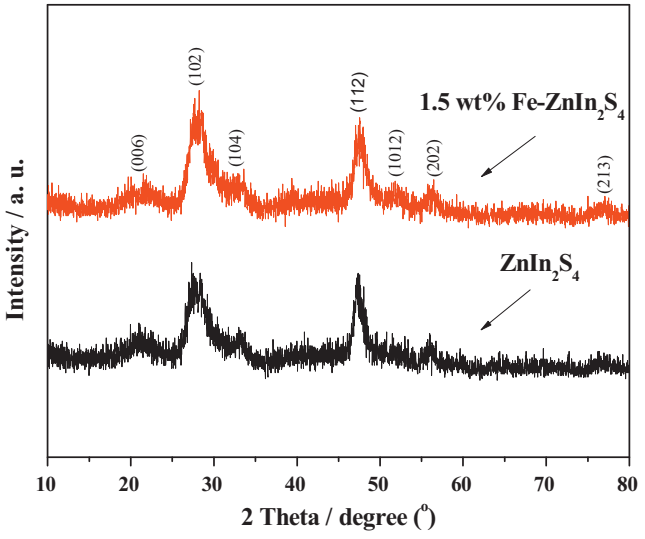

Fig. 3. XRD patterns of the as-prepared $ZnIn_2S_4$ and 1.5 wt% Fe-$ZnIn_2S_4$ catalysts.

3.1.3. FT-IR spectroscopy

The FT-IR spectra of pristine $ZnIn_2S_4$ and Fe-doped $ZnIn_2S_4$ in the range of 400–2000 cm^{-1} are shown in Fig. 4. The bands at ~1610 cm^{-1} and ~1396 cm^{-1} for all the samples probably corresponded to the surface absorbed water molecules and hydroxyl groups [4]. The IR bands in the range of 900–1200 cm^{-1} were characteristic for of C—O in residual solvent. The Fe-doped $ZnIn_2S_4$ composite presented a weak peak at 400–500 cm^{-1}, which might be related to the Fe in the composite catalyst. The bands at ~680–690 cm^{-1} and ~460–490 cm^{-1} were ascribable to β-FeOOH, respectively representing the deformation vibration of —OH and Fe—O stretching vibrations [24,25]. The oxidation of the zero valence Fe was common when exposed in air, and FeOOH was a common product.

3.1.4. BET surface area

Fig. 5 showed the nitrogen adsorption–desorption isotherms of as-prepared $ZnIn_2S_4$, R-$ZnIn_2S_4$ ($ZnIn_2S_4$ without Fe, treated by $NaBH_4$) and 1.5 wt% Fe-$ZnIn_2S_4$ samples. The nitrogen adsorption–desorption isotherms were characteristic of a type IV isotherm with a hysteresis loop which indicated the existence of mesoporous structures in the samples. The corresponding pore size distribution curve (inset, BJH method) showed an average pore size at 3–5 nm. The BET specific surface areas of the $ZnIn_2S_4$, 1.5 wt%

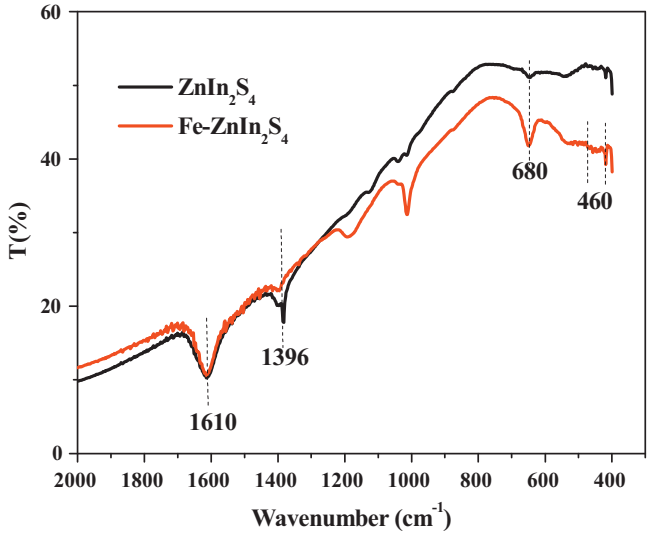

Fig. 4. FT-IR spectra of the prepared $ZnIn_2S_4$ and Fe-doped $ZnIn_2S_4$ samples.

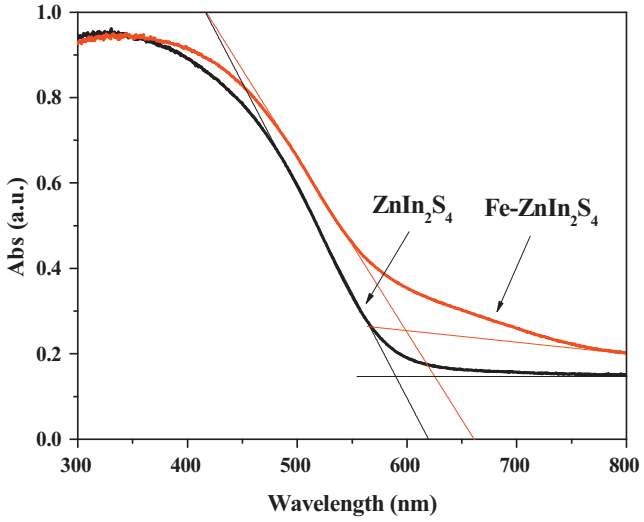

Fig. 6. UV–vis diffuse reflectance spectra of $ZnIn_2S_4$ and 1.5 wt% Fe-$ZnIn_2S_4$.

Fe-$ZnIn_2S_4$ and R-$ZnIn_2S_4$ were 70.9, 58.4 and 27.6 $m^2\ g^{-1}$, respectively. The decrease of the specific surface areas of Fe-$ZnIn_2S_4$ and R-$ZnIn_2S_4$ was 17.6% and 61.1%, respectively, comparing with $ZnIn_2S_4$, indicating the effect of chemical reduction by $NaBH_4$ in significantly decreasing the specific surface area. Depositing ferrous ion can deplete most of the $NaBH_4$ and reduce its destructive effect to $ZnIn_2S_4$, so the specific surface area of Fe-doped $ZnIn_2S_4$ was larger than that of R-$ZnIn_2S_4$. The decrease of the specific surface area for Fe-doped $ZnIn_2S_4$ was attributed to the excess $NaBH_4$.

3.1.5. Catalyst optical properties

The influence of doping nanoscale zerovalent iron on the optical properties was shown in the UV–vis diffuse reflectance spectra in Fig. 6. Both had wide range absorbency from UV to visible region and intense visible-light absorption. The absorption edge of 1.5 wt% Fe-$ZnIn_2S_4$ red-shifted slightly comparing to the $ZnIn_2S_4$. The onset of the absorption edges of the $ZnIn_2S_4$ and Fe-$ZnIn_2S_4$ were at 585 nm and 605 nm and the corresponding band gaps calculated from the onset of the absorption edges [26] were 2.12 eV and 2.05 eV, respectively. The addition of Fe narrowed the band gap and increased light absorption, which may increase the yield of the photogenerated electron–hole pairs and improve the photocatalytic efficiency. Methylene blue (MB), an indicator contaminant, was used to evaluate the photocatalytic activity of the as-prepared catalysts under visible light. $ZnIn_2S_4$ and Fe-doped $ZnIn_2S_4$ all exhibited outstanding adsorption capacity for MB and ~90% of MB was removed after 2.0 h adsorption (Supplementary data, Fig. S2a). When $ZnIn_2S_4$ was doped with Fe, the photocatalytic activity of Fe-$ZnIn_2S_4$ was increased because of the increased visible-light absorption. When the amount of doped Fe^0 was 0.5 wt%, the catalyst exhibited outstanding photocatalytic activity and 100 ml of 50 ppm MB was nearly colorless after 2 h irradiation under visible light (Supplementary data, Fig. S2b), which was in good agreement with the previous literatures [26]. As Fe loadings increased further, the photodegradation efficiency decreased because of the increased agglomeration of Fe^0 on the catalyst surface, which decreased the effective active site for the adsorption of MB (Supplementary data, Fig. S2a). Moreover, excess Fe^{2+} on the catalyst surface can react with both photo-generated electrons and holes and may serve as recombination center. Considering the photocatalytic activity of the catalyst, the 0.5 wt% Fe-$ZnIn_2S_4$ was selected for further investigation.

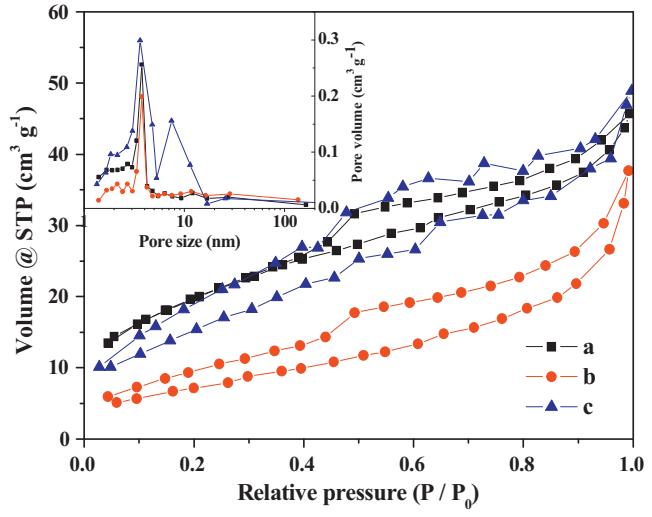

Fig. 5. Nitrogen adsorption–desorption isotherms and the pore size distribution plots (inset) of $ZnIn_2S_4$, R-$ZnIn_2S_4$ and Fe-$ZnIn_2S_4$: (a) $ZnIn_2S_4$, (b) R-$ZnIn_2S_4$ ($ZnIn_2S_4$ treated with $NaBH_4$), (c) 1.5 wt% Fe-$ZnIn_2S_4$.

3.2. Photocatalytic debromination of 2,4,6-tribromophenol

Though the prepared Fe-$ZnIn_2S_4$ has a broad absorption in the visible region, it is very difficult to destroy the C—Br in 2,4,6-tribromophenol because of the strong bond energy of C—Br bond (349.4 ± 10.5 kJ/mol). 95% 2,4,6-TBP was removed by Fe-$ZnIn_2S_4$ under visible irradiation, but the debromination efficiency was very low (data not shown), which did not meet the intended purpose to reduce the toxicity of 2,4,6-TBP. In order to destroy the C—Br bond and reduce the toxic by-products, a 20 W germicidal low-pressure mercury lamp with main wavelength of 254 nm (the light intensity was 297 μW/cm^2) was used. Control tests with $ZnIn_2S_4$ and 0.5 wt% Fe-$ZnIn_2S_4$ under UV light and/or in the dark and the direct photolysis of 2,4,6-TBP were conducted.

The results (Fig. 7) showed that 84% 2,4,6-TBP was removed by $ZnIn_2S_4$ after 1 h adsorption in the dark, while, the adsorption capacity decreased (54% 2,4,6-TBP was removed) with Fe doping, which was probably related to the morphology of the catalysts. The micro-peony with nano-lamella petals of the as-prepared $ZnIn_2S_4$ might be beneficial to the adsorption of 2,4,6-TBP. The lamellar structure microsphere was destroyed by chemical reduction,

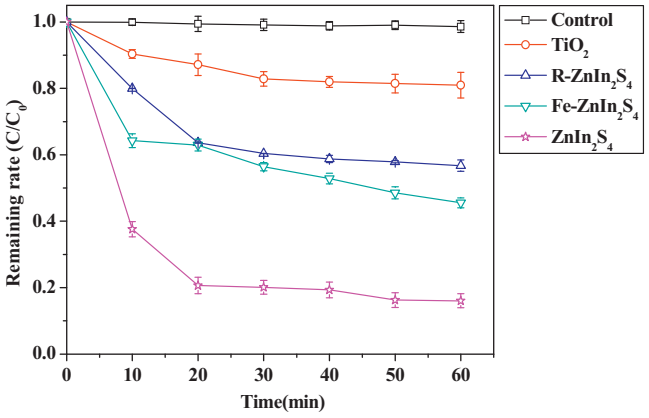

Fig. 7. The adsorption removal of 2,4,6-TBP in the dark by TiO_2, $ZnIn_2S_4$, R-$ZnIn_2S_4$ and 0.5 wt% Fe-$ZnIn_2S_4$ ([2,4,6-TBP]$_0$ = 0.12 mmol, pH 6.89, catalyst dosage = 0.5 g l^{-1}).

which might be detrimental to the adsorption of 2,4,6-TBP. The adsorption capacity of R-$ZnIn_2S_4$ (reduced by $NaBH_4$) decreased a lot and only 43% 2,4,6-TBP was removed after 1 h adsorption. The adsorption capacity was in accordance with the BET surface area of the as-prepared catalysts. Though the chemical reduction caused the decrease in adsorption of 2,4,6-TBP, the photocatalytic degradation of 2,4,6-TBP was enhanced by Fe deposition. Both $ZnIn_2S_4$ and Fe-$ZnIn_2S_4$ exhibited excellent photocatalytic activity and the 2,4,6-TBP cannot be detected after 8 min irradiation (Fig. 8). For comparison, the parallel degradation of 2,4,6-TBP was investigated in the presence of the same quantity of TiO_2 (P25) and 0.5 wt% Fe-TiO_2. The conversion efficiency of 2,4,6-TBP by TiO_2 (P25) and 0.5 wt% Fe-TiO_2 was 85% and 95% after 1 h reaction, respectively (Fig. 8). 98% 2,4,6-TBP was removed by direct photolysis, but this was contributed to the preliminary degradation. The UV–vis spectral of direct photolysis had an intense absorption at 204 nm (Supplementary data, Fig. S3) which corresponded to the E_2 absorption band of benzene, which demonstrated that the benzene ring was not destroyed after irradiation 1 h under UV light. The hypsochromic shift of the absorption band was presumed to the formation of quinones intermediates (the aqueous solution was light brown).

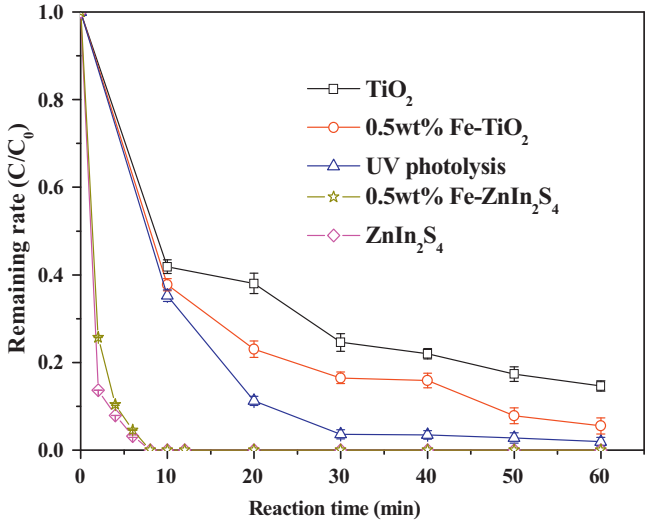

Fig. 8. Photodebromination of 2,4,6-TBP by TiO_2, 0.5 wt% Fe-TiO_2, $ZnIn_2S_4$ and 0.5 wt% Fe-$ZnIn_2S_4$ ([2,4,6-TBP]$_0$ = 0.12 mmol, pH 6.89, catalyst dosage = 0.5 g l^{-1}, 20 W low-pressure mercury lamp (light intensity was 297 μW/cm^2)).

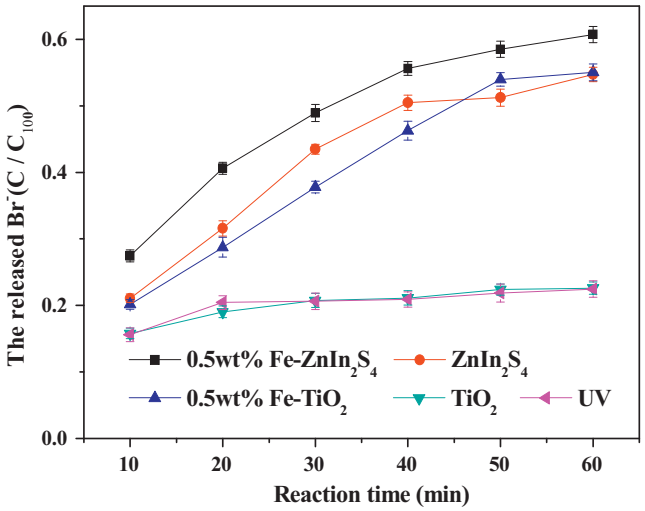

Fig. 9. The released Br^- concentration for different catalysts (C_{100} of bromide was determined as the Br^- concentration at 100% debromination and C represented the released bromide concentration).

The debromination of 2,4,6-TBP by photocatalysts in the presence of UV light was described by pseudo-first-order rate equation:

$$\frac{dC}{dt} = -K_r C \quad (1)$$

where, "C" is the aqueous phase concentration of 2,4,6-TBP (mg l^{-1}). "K_r" is the pseudo-first-order rate constant (min^{-1}) which can be determined by plotting $\ln(C_t/C_0)$ versus reaction time t (min). At the start of photocatalytic reaction, the substrate concentration was marked as C_0. The pseudo-first-order rate constants for 2,4,6-TBP debromination by TiO_2 (P25), Fe-TiO_2, $ZnIn_2S_4$ and Fe-$ZnIn_2S_4$ were 0.022 min^{-1}, 0.0369 min^{-1}, 0.362 min^{-1} and 0.435 min^{-1}, respectively, which was consistent with their conversion efficiencies (Fig. 8).

Bromide ion (Br^-) release is an indicator of debromination of 2,4,6-TBP. Measurement of the yield of bromide ion intermediate is necessary to compare different methods and catalysts in terms of conversion efficiency and by-product toxicity. The C/C_{100} ratios of Br^- for different catalysts were shown in Fig. 9. C_{100} of bromide was determined here as the Br^- concentration at 100% debromination and C represented the released bromide concentration. Doping zero valent nanoparticles to the catalysts played an important role in debromination. After 1 h photocatalytic reaction by Fe-$ZnIn_2S_4$, the released Br^- concentration was 17.6 mg l^{-1} corresponding 61% debromination, which was 1.11 and 2.69 times higher than $ZnIn_2S_4$ and TiO_2 (P25), respectively. Thirty-two percent higher bromide was released by Fe-TiO_2, compared with TiO_2 (P25).

TOC is an important indicator to judge the mineralization degree of the organic pollutants. After the reduction and oxidation debromination of 2,4,6-TBP, the hydroxylation and cleavage of the benzene ring followed and the generated carbon species were subsequently degraded, which led to complete mineralization. Doping Fe^0 not only improved the debromination efficiency but also enhanced the mineralization of 2,4,6-TBP for both TiO_2 and $ZnIn_2S_4$. TOC removal rates (Fig. 10) achieved by direct UV photolysis, TiO_2, 0.5 wt% Fe-TiO_2, $ZnIn_2S_4$ and 0.5 wt% Fe-$ZnIn_2S_4$ were 6%, 14%, 36%, 40% and 47%, respectively after 1 h reaction. Although the complete elimination of the TOC may not be achieved within the 1 h test period, especially for the persistent organic pollutants 2,4,6-TBP, the conversion and the debromination of 2,4,6-TBP revealed a substantial degradation to simpler smaller compounds.

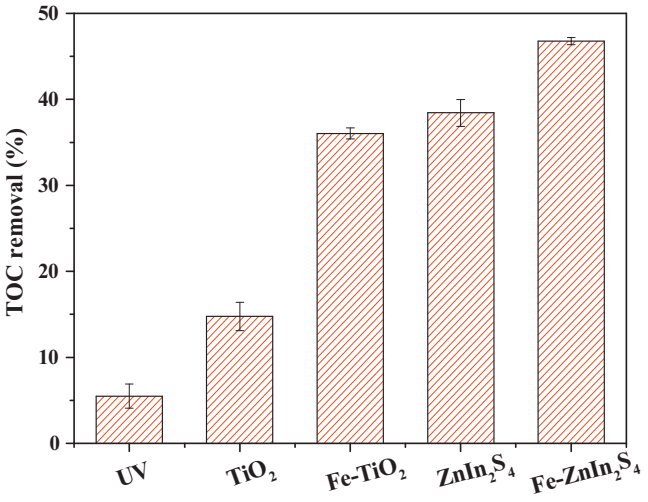

Fig. 10. TOC removal by different catalysts after 1 h reaction ([2,4,6-TBP]$_0$ = 0.12 mmol, pH 6.89, catalyst dosage = 0.5 g l^{-1}, 20 W low-pressure mercury lamp).

3.3. Debromination pathway of 2,4,6-TBP by Fe^0-$ZnIn_2S_4$

For degradation pathway analysis, the debromination of 2,4,6-TBP by 0.5 wt% Fe-$ZnIn_2S_4$ was carried out under UV irradiation (the light intensity was 297 μW/cm^2), the intermediate products resulting from 2,4,6-TBP photocatalytic degradation at 10 min, 30 min and 60 min were analyzed using HPLC-ESI MS. According to results listed in Table 1, three main intermediate product ions at *m*/*z* 187, *m*/*z* 250.7 and *m*/*z* 266.8 were detected after 10 min photocatalytic debromination, which probably corresponded to 2-bromo-1,4-benzoquinone, 2,4-dibromophenol and/or 2,6-dibromophenol and 2,6-dibromo-p-benzoquinone, respectively. The characteristic peak of 2,4,6-TBP at *m*/*z* 328.8 was not detected and 100% 2,4,6-TBP was transformed within 10 min. The results revealed that 2,4,6-TBP was completely decomposed and simultaneously transformed to the detected main intermediates. The relative intensity of the extracted ion chromatography changed with the irradiation time (Table 1). The relative intensity of 2,6-dibromo-p-benzoquinone decreased along with the irradiation time and the relative intensity of 2-bromo-1,4-benzoquinone increased firstly and then decreased within 60 min. The species of 2,4-dibromophenol and/or 2,6-dibromophenol increased within the 60 min irradiation and a new ion peak of *m*/*z* 172.9 corresponding to 2-bromophenol and/or 4-bromophenol was detected after irradiation 30 min. It has been proposed that quinones were formed as the main intermediates during the oxidative dehalogenation of 2,4,6-trichlorophenol by Fe-porphyrin [27] and hemin–acrylic copolymer [28] and bromophenols (tri-BBPA, di-BBPA, mono-BBPA and BPA) were the major intermediates during the reductive debromination of TBBPA over iron-silver bimetallic nanoparticles [29]. On the basis of the identified intermediates, we proposed that the degradation of 2,4,6-TBP by Fe^0-$ZnIn_2S_4$ under UV irradiation started via both oxidative debromination (hydroxylation) and reductive debromination. Additionally, the quinones (2,6-dibromo-p-benzoquinone and 2-bromo-1,4-benzoquinone) made up a large part of the intermediates, which indicated that the oxidative debromination played a leading role in the photocatalytic debromination of 2,4,6-TBP.

Table 1
The debromination intermediates detected by LC MS at the reaction time of 10 min, 30 min and 60 min ([2,4,6-TBP]$_0$ = 0.12 mmol, pH 6.89, 0.5 wt% Fe-$ZnIn_2S_4$, dosage = 0.5 g l^{-1}).

Reaction time	*m*/*z*	Relative intensity	Proposed compound
0 min	328.8	2.05×10^6	2,4,6-Tribromophenol
10 min	187	3.2×10^4	2-Bromo-1,4-benzoquinone
	250.7	4.5×10^4	2,4-Dibromophenol2,6-Dibromophenol
	266.8	5.5×10^5	2,6-Dibromo-p-benzoquinone
30 min	172.9	1.6×10^4	2-Bromophenol or 4-bromophenol
	187	1.3×10^5	2-Bromo-1,4-benzoquinone
	250.7	6.0×10^4	2,4-Dibromophenol2,6-Dibromophenol
	266.8	4.0×10^5	2,6-Dibromo-p-benzoquinone
60 min	172.9	2.4×10^4	2-Bromophenol or 4-bromophenol
	187	1.1×10^5	2-Bromo-1,4-benzoquinone
	250.7	1.1×10^5	2,4-Dibromophenol2,6-Dibromophenol
	266.8	3.0×10^5	2,6-Dibromo-p-benzoquinone

According to the previously proposed mechanisms for degradation of other aromatic organic molecules [1,3,27–29] and the experimental results in this study, the photodegradation pathway of 2,4,6-TBP was proposed in Scheme 1, which outlined both oxidative and reductive debromination. On one hand, 2,4,6-TBP can undergo reductive debromination by ZVI NPs to produce less-brominated homologues (DBP or BP) [8] and ZVI NPs were transformed to Fe^{2+} and/or Fe^{3+} (Eq. (1)). Moreover, the photocatalytic debromination was enhanced via an increased supply of •OH from the Fenton-like reaction induced by the photolysis of Fe^0 (Eq. (2)) and H_2O (Eq. (3)) under UV light irradiation [30]. The generated Fe^{2+} (Eqs. (1) and (2)) acted as a Fenton system [31] (Eq. (5)) together with the H_2O_2 produced by the HO_2 radical which was formed from the photolysis of H_2O (Eqs. (3) and (4)) to accelerate the oxidation reaction.

$$Fe^0 + 2H^+ + \text{R-Br} \rightarrow \text{R-H} + Br^- + Fe^{2+} \quad (2)$$

$$Fe^0 + h\nu \rightarrow Fe^{2+} + 2e^-; \quad Fe^{2+} + h\nu \rightarrow Fe^{3+} + e^- \quad (3)$$

$$2H_2O + h\nu (\leq 698\,\text{nm}) \rightarrow HO_2 + 3H^+ \quad (4)$$

$$HO_2 (^\bullet O_2^-) + 3H^+ \rightarrow H_2O_2 + H_2 \quad (5)$$

$$Fe^{2+} + H_2O_2 \rightarrow Fe(OH)^{2+} + {}^\bullet OH \quad (6)$$

On the other hand, the holes generated on $ZnIn_2S_4$ by UV irradiation (Eq. (6)) can be used to directly oxidize the 2,4,6-TBP and a part of the generated-electrons can react with the dissolved oxygen to form $^\bullet O_2^-$ which further generated H_2O_2 and •OH (Eqs. (7)–(9)) to accelerate the oxidation reaction of 2,4,6-TBP. And another part of the generated-electrons can be trapped by the two half reactions of Fe^{3+}/Fe^{2+} and Fe^{2+}/Fe^0, which prevented the recombination of electrons and holes and realized the positive cycle of Fe^0.

$$Fe^0\text{-}ZnIn_2S_4 + h\nu \rightarrow h^+ + e^- \quad (7)$$

$$O_2 + e^- \rightarrow O_2^- \quad (8)$$

$$2e^- + O_2 + 2H^+ \rightarrow H_2O_2 \quad (9)$$

$$H_2O_2 + {}^\bullet O_2^- \rightarrow {}^\bullet OH + OH^- + O_2 \quad (10)$$

The synergistic effect of Fe^0 and $ZnIn_2S_4$ under UV irradiation can produce large amounts of active species with strong oxidation capacity which contribute greatly to oxidative debromination of 2,4,6-TBP. The photocatalyst $ZnIn_2S_4$, served as the support of Fe^0 nanoparticles, can effectively decrease the agglomeration of ZVI NPs and improve the reactivity and stability of ZVI NPs. At the same time, the photo-generated electrons and holes can be separated effectively due to the two half reactions of Fe^{3+}/Fe^{2+} and Fe^{2+}/Fe^0.

3.4. The stability and durability of Fe^0-$ZnIn_2S_4$ composite

In order to evaluate the stability and recycling of the catalyst, two round seven-cycle debromination experiments were

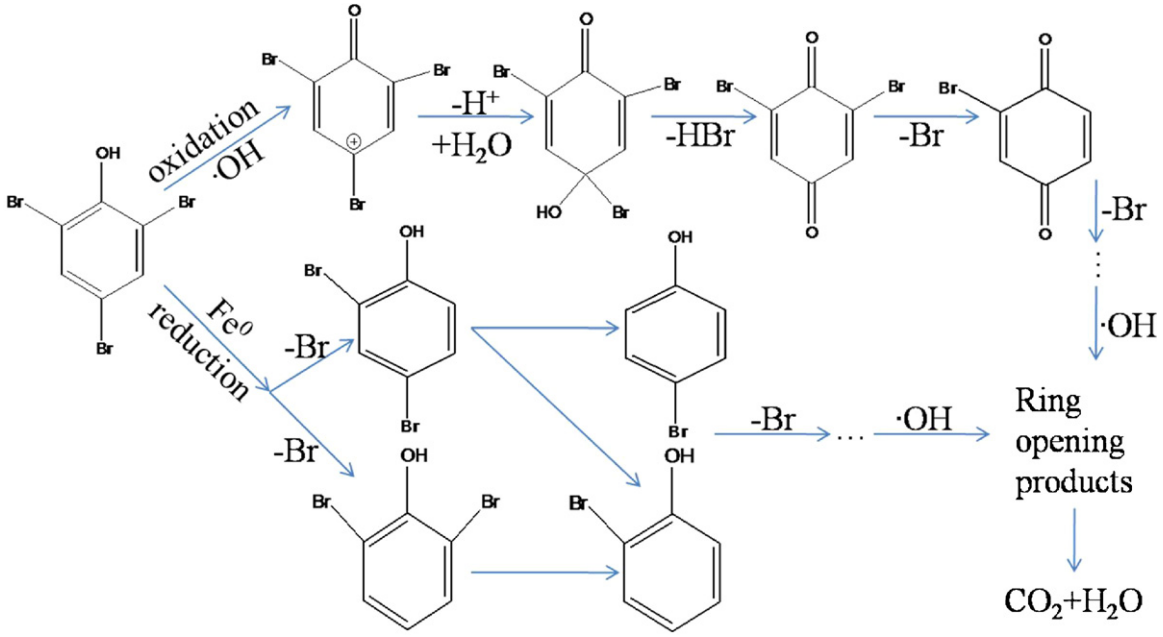

Scheme 1. Proposed debromination pathway of 2,4,6-TBP by Fe^0-$ZnIn_2S_4$.

conducted. When the first round seven-cycle experiment was completed, the catalyst was collected in a 10 ml sampling bottle to start another seven-cycle experiment after two months. The catalyst of Fe-$ZnIn_2S_4$ showed highly photocatalytic activity after 7 cycles and 2,4,6-TBP was completely removed. Though the content of released Br^- decreased a little, it can be maintained more than 55% (Fig. 11). 2,4,6-TBP was also completely removed after another 7 cycles and the Br^- formation was still maintained more than 55%. This implied that long-time storage would not affect the photocatalytic activity and the catalyst could be reused for many times without significant loss in photocatalytic activity. The outstanding stability of the Fe-$ZnIn_2S_4$ composite was benefited from the synergistic effect of Fe^0 and $ZnIn_2S_4$. At a low Fe loading, photo-generated holes and electrons were well separated, as the electrons generated on $ZnIn_2S_4$ can be trapped for the reduction of Fe^{3+} or Fe^{2+} which were formed on the Fe surface by chemical debromination of 2,4,6-TBP and/or photolysis of Fe^0. This might prevent the formation of the oxidation layer and reduce the recombination of photo-generated holes and electrons. Moreover, enough electrons could be produced by $ZnIn_2S_4$ under UV irradiation and Fe^{3+} or Fe^{2+} on the Fe surface could be reduced in a timely fashion, therefore, the Fe^{3+} or Fe^{2+} would not accumulate on Fe surface and prevent the formation of a surface passivation layer. Furthermore, $ZnIn_2S_4$ with a higher conduction band than TiO_2, thus can provide electrons for the better reduction of Fe^{3+} and Fe^{2+}. This was expected to prevent the formation of oxide layer on the Fe^0 surface and to maintain the reactivity of Fe^0 during the debromination process. It is further anticipated that the combination of Fe-$ZnIn_2S_4$ photocatalyst with the membrane separation process may be feasible for real application in treatment of recalcitrant contaminates.

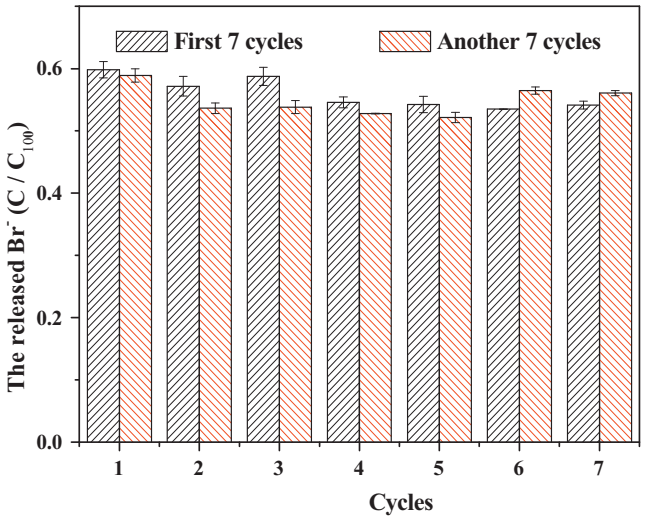

Fig. 11. The released Br^- concentration during the seven cyclic experiment (another 7 cycles was carried out after two months).

4. Conclusions

Fe doped $ZnIn_2S_4$ reduced the band gap of $ZnIn_2S_4$ and increased the degradation efficiency of 2,4,6-TBP because of the increased light absorption. Compared with TiO_2 (P25) and $ZnIn_2S_4$, Fe doped $ZnIn_2S_4$ catalyst was more efficient in debromination and total organic carbon (TOC) removal. SEM and BET analysis indicated that the lamellar structure microsphere of $ZnIn_2S_4$ was destroyed by $NaBH_4$ chemical reduction and resulted in adsorption capacity reduction. Fe doped $ZnIn_2S_4$ kept the large BET surface area because that depositing ferrous ion can deplete most of the $NaBH_4$ and reduce its destructive effect to $ZnIn_2S_4$. LC MS analysis of intermediates revealed that both reductive and oxidative debromination were involved in the photodegradation of 2,4,6-TBP over Fe-$ZnIn_2S_4$. The repeated tests indicated that Fe doped $ZnIn_2S_4$ catalyst could be reused for many times without significant loss in photocatalytic activity.

Appendix A. Supplementary data

Supplementary data associated with this article can be found, in the online version, at http://dx.doi.org/10.1016/j.apcatb.2012.09.007.

References

[1] T. Yamada, Y. Takahama, Y. Yamada, Bioscience, Biotechnology, and Biochemistry 72 (2008) 1264–1271.

[2] A. Konstantinov, D. Bejan, N.J. Bunce, B. Chittim, R. McCrindle, D. Potter, C. Tashiro, Chemosphere 72 (2008) 1159–1162.
[3] J. Xu, W. Meng, Y. Zhang, L. Li, C. Guo, Applied Catalysis B: Environmental 107 (2011) 355–362.
[4] Y. Li, F. Jiang, Q. Xiao, R. Li, K. Li, M. Zhang, A. Zhang, S. Sun, Y. Liu, Applied Catalysis B: Environmental 101 (2010) 118–129.
[5] W.P. Hsieh, J.R. Pan, C. Huang, Y.C. Su, Y.J. Juang, Science of The Total Environment 408 (2010) 672–679.
[6] G.K. Parshetti, R. Doong, Applied Catalysis B: Environmental 100 (2010) 116–123.
[7] G.K. Parshetti, R. Doong, Water Research 45 (2011) 4198–4210.
[8] S. Choe, S. Lee, Y. Chang, K. Hwang, J. Khim, Chemosphere 42 (2001) 367–372.
[9] S. Xiao, M. Shen, R. Guo, S. Wang, X. Shi, Journal of Physical Chemistry C 113 (2009) 18062–18068.
[10] B. Sunkara, J. Zhan, J. He, G.L. McPherson, G. Piringer, V.T. John, Applied Materials & Interfaces 2 (2010) 2854–2862.
[11] V. Smuleaca, R. Varmab, S. Sikdarb, D. Bhattacharyyaa, Journal of Membrane Science 379 (2011) 131–137.
[12] L. Liu, F. Chen, F. Yang, Y. Chen, J. Crittenden, Chemical Engineering Journal 181 (2012) 189–195.
[13] L. Liu, F. Chen, F. Yang, Separation and Purification Technology 70 (2009) 173–178.
[14] X. Gou, F. Cheng, Y. Shi, L. Zhang, S. Peng, J. Chen, P. Shen, Journal of the American Chemical Society 128 (2006) 7222–7229.
[15] K.W. Cheng, C.J. Liang, Solar Energy Materials and Solar Cells 94 (2010) 1137–1145.
[16] M. Li, J. Su, L. Guo, International Journal of Hydrogen Energy 33 (2008) 2891–2896.
[17] H. Yu, X. Quan, Y. Zhang, N. Ma, S. Chen, H. Zhao, Langmuir 24 (2008) 7599–7604.
[18] X. Hu, J.C. Yu, J. Gong, Q. Li, Crystal Growth and Design 7 (2007) 2444–2448.
[19] Z. Lei, W. You, M. Liu, G. Zhou, T. Takata, M. Hara, K. Domen, C. Li, Chemical Communications 214 (2003) 2–2143.
[20] S. Shen, L. Zhao, Z. Zhou, L. Guo, Journal of Physical Chemistry C 112 (2008) 16148–16155.
[21] Z. Chen, D. Li, W. Zhang, Y. Shao, T. Chen, M. Sun, X. Fu, Journal of Physical Chemistry C 113 (2009) 4433–4440.
[22] B. Chai, T. Peng, P. Zeng, X. Zhang, X. Liu, Journal of Physical Chemistry C 115 (2011) 6149–6155.
[23] Z. Chen, D. Li, W. Zhang, C. Chen, W. Li, M. Sun, Y. He, X. Fu, Inorganic Chemistry 47 (2008) 9766–9772.
[24] S. Musić, G.P. Santana, G. Šmit, V.K. Garg, Journal of Alloys and Compounds 278 (1998) 291–301.
[25] C. Wei, Z. Nan, Macromolecular Chemistry and Physics 127 (2011) 220–226.
[26] F. Fang, L. Chen, Y.B. Chen, L.M. Wu, Journal of Physical Chemistry C 114 (2010) 2393–2397.
[27] K.C. Christoforidis, E. Serestatidoua, M. Louloudib, I.K. Konstantinoua, E.R. Milaevac, Y. Deligiannakisa, Applied Catalysis B: Environmental 101 (2011) 417–424.
[28] G.D. Díaz, M.C. García, M.C.B. López, M.J. Lobo-Castañón, A.J.M. Ordieres, P.T. Blanco, Applied Catalysis B: Environmental 96 (2010) 51–56.
[29] S. Luo, S. Yang, X. Wang, C. Sun, Chemosphere 79 (2010) 672–678.
[30] H.S. Son, J.K. Im, K.D. Zoh, Water Research 43 (2009) 1457–1463.
[31] J. Li, Z. Ai, L. Zhang, Journal of Hazardous Materials 164 (2009) 18–25.